Assessment of the Geometric and Temporal Errors Associated with Airborne Doppler Radar Measurements of a Convective Storm

PETER S. RAY

Department of Meteorology and Supercomputer Computations Research Institute, Florida State University, Tallahassee, Florida

MARY STEPHENSON

Control Data Corporation and Supercomputer Computations Research Institute, Tallahassee, Florida

(Manuscript received 28 December 1988, in final form 22 July 1989)

ABSTRACT

On 20 April 1984, the NOAA WP-3D aircraft, equipped with a Doppler radar in its tail, flew around a growing thunderstorm near Norman, Oklahoma. Doppler wind data was collected as the airplane flew six legs around the storm. During this time, the National Severe Storms Laboratory (NSSL) dual-Doppler network collected data on the same storm. Different combinations of synthesis techniques were examined employing direct and pseudo-dual-Doppler observations from aircraft alone, and combinations of aircraft and ground-based Doppler radar. The effect of temporal resolution errors was assessed and related to uncertainties caused by geometric configuration. For this system, it was found that although the aircraft did provide useful data by extending the analysis to the region between the ground-based radars, the contribution was limited by the rapid evolution of the storm. Greater utility may generally be found for storms that evolve less rapidly.

1. Introduction

Ground-based Doppler radars have been used in meteorological studies for many years. Their usefulness in studying the winds within convective storms, microbursts, and other phenomena has already been established. Recently, scientists have begun exploring the extension of proven ground-based Doppler analysis techniques to the study of airborne Doppler radar data. This has been made possible by the installation of a 3-cm Doppler radar in the National Oceanic and Atmospheric Administration (NOAA) WP-3D research aircraft.

Already, airborne Doppler radar has been used in the study of microbursts (e.g., Mueller and Hildebrand 1985), sea breeze storms (e.g., Ray et al. 1985), hurricanes (e.g., Marks and Houze 1987), and other convective storms (e.g., Hildebrand and Mueller 1985). Other assessments of the airborne Doppler concept include those of Lhermitte (1971), Jorgensen et al. (1983), and Ray and Jorgensen (1987). One obvious advantage of airborne Doppler radar is the mobility of the airplane. This allows the researcher to collect data on storms which are out of the range of land-based Dopplers (e.g., ocean storms) and enables data collection over the entire length of the evolution of a moving storm. Airborne Doppler radar can also provide better spatial resolution than ground-based Doppler radars and can collect data on larger storms than fixed radars.

An airborne Doppler study of a convective sea breeze storm off the coast of Florida was discussed in Ray et al. (1985). They compared expected errors from two different analysis techniques for different flight paths. The so-called "direct" method requires data at each grid point from at least three different radars or flight legs. The overdetermined dual-Doppler method uses least squares techniques to solve for the horizontal wind components and integration of the continuity equation to solve for the vertical velocity component. They related the airborne collection procedure to an analogous data collection geometry for ground-based radars. Both analysis techniques produced similar wind fields. No clear guidelines as to which solution technique to use under different circumstances could be formulated. For each geometrical configuration, different parts of the analysis area were better suited to each synthesis technique.

In the first of two papers, Hildebrand and Mueller (1985) compared results obtained from dual airborne Doppler radar, dual ground-based Doppler radar, and combined airborne and ground-based Doppler radar analyses. The second paper (Mueller and Hildebrand 1985) evaluated the use of an airborne Doppler in combination with two ground-based Dopplers. These

Corresponding author address: Dr. Peter Ray, Department of Meteorology, Florida State University, Tallahassee, FL 32306.

studies were conducted as part of the Joint Airport Weather Studies (JAWS) experiment in June 1982. A severe microburst-producing storm was observed by the WP-3D aircraft while it was in the range of two ground-based radars. All of the dual-Doppler radar analyses showed good agreement in wind field structure and magnitude. Observed differences appeared to be due to known problems with airborne Doppler radar data collection, e.g., long collection periods, inaccuracies in antenna pointing angle, and poor resolution in the along-track directions. Additional differences were introduced through uncertainty in the ground-based radar measurements. This could arise from the geometry of the radars with respect to the observing point. The addition of the airborne Doppler data to a ground-based dual Doppler radar dataset was shown to improve the analysis results. The ease of using the aircraft's radar in a vertically pointing mode improved the ability to calculate vertical velocities. The airborne Doppler radar could also be used to measure divergence at the storm boundaries more accurately and easily, resulting in improved analysis results. Drawbacks of the airborne Doppler radar in these situations are low elevation angle, coarse horizontal resolution, low sensitivity, and poor terminal velocity estimates. Overall, airborne Doppler radars were seen to improve the ability to study convective storms in many instances.

2. Airborne Doppler characteristics

The NOAA WP-3D aircraft has a 3.2-cm Doppler radar located in the tail of the aircraft. This radar scans vertically in a plane that is normal to the flight track, resulting in a helical scan volume (Fig. 1). The aircraft also has a 5-cm incoherent radar in the nose of the aircraft that is pointed in a forward direction and a 5-cm radar underneath the airplane that scans in a nearly horizontal plane. The flight level was 5.2 km MSL and flight speed was approximately 140 m s^{-1}. The X-band Doppler radar on board the aircraft has a pulse repetition time of 625 microseconds, and a Nyquist velocity of 12.7 m s^{-1}. The horizontal and vertical beamwidths are 1.34° and 1.9°, respectively. There were 256 gates along a beam, with gate spacing of 0.150 km, resulting in an effective range of 40 km. The pulse volume depth was 0.15 km. Additional details about the radar can be found in Jorgensen (1983).

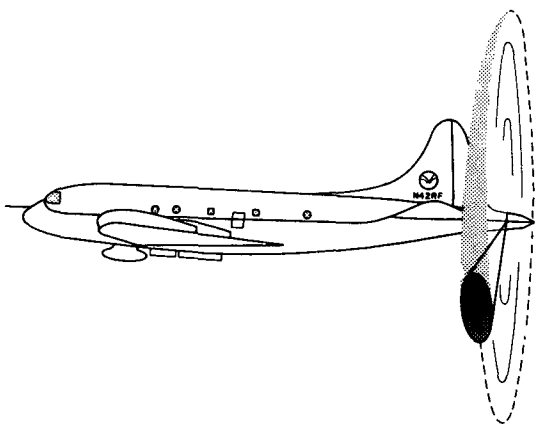

FIG. 1. Schematic of the NOAA Orion P-3 aircraft showing the helical scan surface of the tail radar.

In ground-based radar terminology, azimuth (θ) is the angle of the radar beam measured clockwise from north and elevation (ϕ) is the angle of the radar beam measured positive up from the horizontal. The azimuth and elevation angles in the data taken from the aircraft are reversed from these conventional ground-based radar definitions. The airborne radar data is manipulated to keep the same frame of reference as that used with ground-based radars. Thus, the maximum volume scan extends in elevation angles from +90° to −90°.

The antenna servo-system of the WP-3D's Doppler radar was designed to keep the scanning plane of the radar beam always aligned perpendicular to the aircraft's track. This is accomplished by adjusting the antenna's azimuth according to procedures outlined in Hildebrand and Mueller (1985). The effect of this automatic correction to the azimuth angle is to ensure that the measured radial winds do not contain any component of the motion of the plane relative to the earth. The component of the aircraft's velocity that contaminates the radial velocity data due to the beam not pointing perpendicular to the aircraft's track is removed in postflight processing according to $V_c = GS \cos\theta$, where V_c is the velocity correction to be subtracted from the radial velocity estimates, GS the aircraft's ground speed, and θ, the angle between the actual azimuth angle and the angle perpendicular to the aircraft's track.

3. Processing and analysis of data

a. Doppler radar processing

The airborne radar data were first corrected for the aircraft roll and vertical velocity. The component of the aircraft's velocity was subtracted from the measured radial velocity. The azimuth and elevation were changed to correspond to standard definitions of these angles. The data was first archived and put in universal format. It was then edited to remove any obvious bad data points, unfold velocities as necessary, and remove noise. As a result of the low Nyquist velocity of the WP-3D data, there was much velocity folding in this data, and it had to be unfolded on every scan of the six flight legs studied here.

The ground-based Doppler radar data were also archived and put in universal format. These radars had a significantly larger Nyquist velocity than the airborne Doppler radar and did not exhibit the widespread ve-

locity folding found in the airborne radar data. Therefore, this data did not require substantial editing.

b. Analysis procedures

All of the analyses presented in this paper used an overdetermined dual-Doppler method (Ray et al. 1980; Ray and Sangren 1983) to solve for the components of the wind field. A minimum of two independent observations of each point in space is required. If a radar is located at (x_i, y_i, z_i) and is observing a point (x, y, z) defined by the radar parameters (R_i, θ_i, ϕ_i) then

$$\frac{u(x-x_i)}{R_i} + \frac{v(y-y_i)}{R_i} + \frac{W(z-z_i)}{R_i} = V_i. \quad (1)$$

The range is given by

$$R_i = [(x-x_i)^2 + (y-y_i)^2 + (z-z_i)^2]^{1/2} \quad (2)$$

and

$$w = W - V_t. \quad (3)$$

Here, V_i is the radial component of the scatterers, V_t is the mean terminal fallspeed of the hydrometeors within the pulse volume as determined by Joss and Waldvogel (1970), and W is the particle fallspeed. The horizontal wind components in the x, y, and z directions are u, v, and w.

In the overdetermined dual-Doppler method, the anelastic equation of continuity,

$$\frac{\partial u}{\partial x} + \frac{\partial v}{\partial y} + \frac{\partial w}{\partial z} - \kappa w = 0 \quad (4)$$

where κ is the negative logarithmic rate of change of mean density with height, is used to close the equation set. Using least-squares techniques, the u and v wind components can be rewritten as

$$u = \frac{\sum R_i V_i (x-x_i) \sum (y-y_i)^2 - \sum R_i V_i (y-y_i) \sum (x-x_i)(y-y_i)}{\sum (x-x_i)^2 \sum (y-y_i)^2 - [\sum (x-x_i)(y-y_i)]^2} + \frac{W[\sum (y-y_i)(z-z_i) \sum (x-x_i)(y-y_i) - \sum (y-y_i)^2 \sum (x-x_i)(z-z_i)]}{\sum (x-x_i)^2 \sum (y-y_i)^2 - [\sum (x-x_i)(y-y_i)]^2} \quad (5a)$$

$$v = \frac{\sum R_i V_i (y-y_i) \sum (x-x_i)^2 - \sum R_i V_i (x-x_i) \sum (x-x_i)(y-y_i)}{\sum (y-y_i)^2 \sum (x-x_i)^2 - [\sum (x-x_i)(y-y_i)]^2} + \frac{W[\sum (x-x_i)(y-y_i) \sum (x-x_i)(z-z_i) - \sum (x-x_i)^2 \sum (y-y_i)(z-z_i)]}{\sum (y-y_i)^2 \sum (x-x_i)^2 - [\sum (x-x_i)(y-y_i)]^2}. \quad (5b)$$

The vertical wind component is found from integration of the continuity equation. Improved estimates of u and v are then found through iteration. In the analyses done for this study, the equation of continuity was integrated downward from a boundary condition of $w = 2$ m s^{-1}, and 2 m s^{-1} was used as an upper boundary condition since it was assumed that the storm is in steady state. For that to be true, the vertical wind must support the hydrometeors at the storm top, otherwise the storm would collapse—as it eventually does. Here 2 m s^{-1} is a reasonable estimate of terminal fallspeed at storm top. The uncertainty in the upper boundary condition is a source of error. The effect of this error, however, is progressively reduced with decreasing height. The lower boundary condition is not any better known, and the effect any error associated with it increases with height. Finally, the velocities were adjusted such that the vertically integrated horizontal divergence was near zero, as outlined in Ray et al. (1980).

A 30 by 30 by 15 km analysis grid was used in all cases. The grid spacing was 1.0 km in every direction. In the ground-based Doppler analyses, each observation (radial velocity and reflectivity) was interpolated to the nearest grid point. Using Cressman weighting, the objective analysis resulted in a grid of radial velocity and reflectivity values for each radar as in Ray et al. (1980). The reflectivity fields from the two radars were averaged together. In the airborne Doppler analysis, each radial of data was treated as a separate radar. For every radial of data collected, the airplane (and thus the radar) was in a different location. Therefore, each point in space would appear to have been observed by many different "radars." In other words, each point from which observations were made was treated as a radar. In the analyses which combined ground-based Doppler data with airborne Doppler data, each ground-based radar was still treated as only one radar. Therefore, each ground-based Doppler was effectively given the same weight as each radial of airborne data. In the airborne analyses, the final reflectivity field consisted of the highest observed value at each point, rather than the average value. This was to mitigate the effects of attenuation.

The storm motion was initially estimated by visually correlating reflectivity features at different times from the ground-based dual-Doppler analyses. The storm

motion velocity vector was estimated to be 21.6 m s^{-1} towards the northeast. Later, the motion was estimated by maximizing the vector wind correlations as outlined in Lamberth (1966), with the storm motion estimated to be 23 m s^{-1}. The vector wind correlation is expressed as

$$R^2 = \frac{S_{u_1}^2(r_{u_1u_2}^2 + r_{u_1v_2}^2 - 2r_{u_1u_2}r_{u_1v_2}r_{u_2v_2})}{(S_{u_1}^2 + S_{v_1}^2)(1 - r_{u_2v_2}^2)} + \frac{S_{v_1}^2(r_{v_1u_2}^2 + r_{v_1v_2}^2 - 2r_{v_1u_2}r_{v_1v_2}r_{u_2v_2})}{(S_{u_1}^2 + S_{v_1}^2)(1 - r_{u_2v_2}^2)} \quad (6)$$

where the r refer to the correlations between the indicated scalar fields. The $S_{u_1}^2$ is the variance of the u component of $\mathbf{V}_1$; similarly for $S_{v_1}^2$. This function is positive definite. The storm motion vector was used to translate the data to the central time used in each analysis via a Galilean transformation. Errors in this estimate can be expected to contribute to errors in the analyses. Rapidly evolving storms such as the one studied here are particularly susceptible to this source of error. The relatively long collection times of airborne Doppler systems mean that temporal changes are a real problem. The analysis techniques rely on the assumption that the observations were made at the same (or nearly the same) time. If the flight legs take too long, then the validity of the results becomes questionable.

4. Data description

The storm center was 15 to 20 km from the aircraft during the analysis period. The data collected by the Norman and Cimarron Doppler radars between 1538 and 1638 CST were archived and analyzed. The center of the storm ranged from about 20 to 40 km from the ground-based Doppler radars over the time of the aircraft data collection. The Norman and Cimarron radars had wavelengths of 10.52 and 10.95 cm and a Nyquist velocity of 28.53 and 35.67 m s^{-1}, respectively. The beamwidths were about 0.84 degrees. Both radars were in PPI mode, collecting data in constant elevation angle sector scans. Nine Doppler analysis times using data from Norman, Cimarron and six flight legs from the airborne Doppler radar were used for this study. The time span extended from 1554 to nearly 1612 CST. The box flight pattern is shown in Fig. 2. The origin, coordinates (0, 0), is the Norman radar location and the + sign is the location of the two ground-based radars for all figures. Each flight leg lasted approximately two minutes. During the time period of the last three flight legs, the storm developed a classic hook echo shape in the reflectivity field. The results presented here will concentrate on that time period.

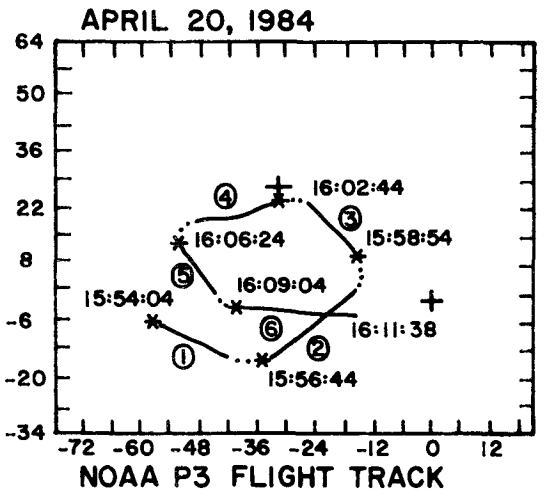

FIG. 2. Map of flight track showing the two ground-based radars. Times are the beginning of legs. Leg number is indicated on the leg. Axes are in km and the Norman and Cimarron radar locations are at coordinates (0.0, 0.0) and (−31.7, 26.6) km, respectively.

5. Results

Horizontal reflectivities and storm relative flow fields as determined by the ground-based Doppler radars for six synthesis times spanning the interval of airborne Doppler radar collection are shown in Fig. 3. The storm was growing and moving rapidly to the northeast during the data collection interval. Maximum reflectivities were in excess of 55 dBZ. A hook echo preceded the occurrence of a tornado reported by ground "chase" teams.

It is possible, in principle, to synthesize wind fields from either airborne data alone, or a combination of airborne radar data and ground-based radar data. A combined airborne and ground-based radar analysis was done using data from the Norman radar and leg 6. This is shown in Fig. 4. A dual airborne Doppler analysis using legs 4 and 5 is shown in Fig. 5. Figure 6 shows the results from using legs 5 and 6, while Fig. 7 comes from an analysis using all three of the last flight legs. All of the figures display the 4 km height level to facilitate comparison.

The sequence of ground-based dual-Doppler analysis results show the rapid speed at which the storm was moving toward the northeast. By 1555 CST (Fig. 3c), an indentation in the echo has become quite deep and the cyclonic circulation is still present. The gradient of reflectivity is very steep on the left-hand side of this circulation. By 1607 (Fig. 3e), there are two cyclonic circulations apparent in addition to a weak anticyclonic circulation. The cyclonic circulation associated with the hooklike reflectivity feature is still there, while another cyclonic pattern has formed immediately to the southeast of the anticyclonic circulation. The storm was producing hail by the time of the last ground-based analysis shown (Fig. 3f, 1612). Unfortunately, due to

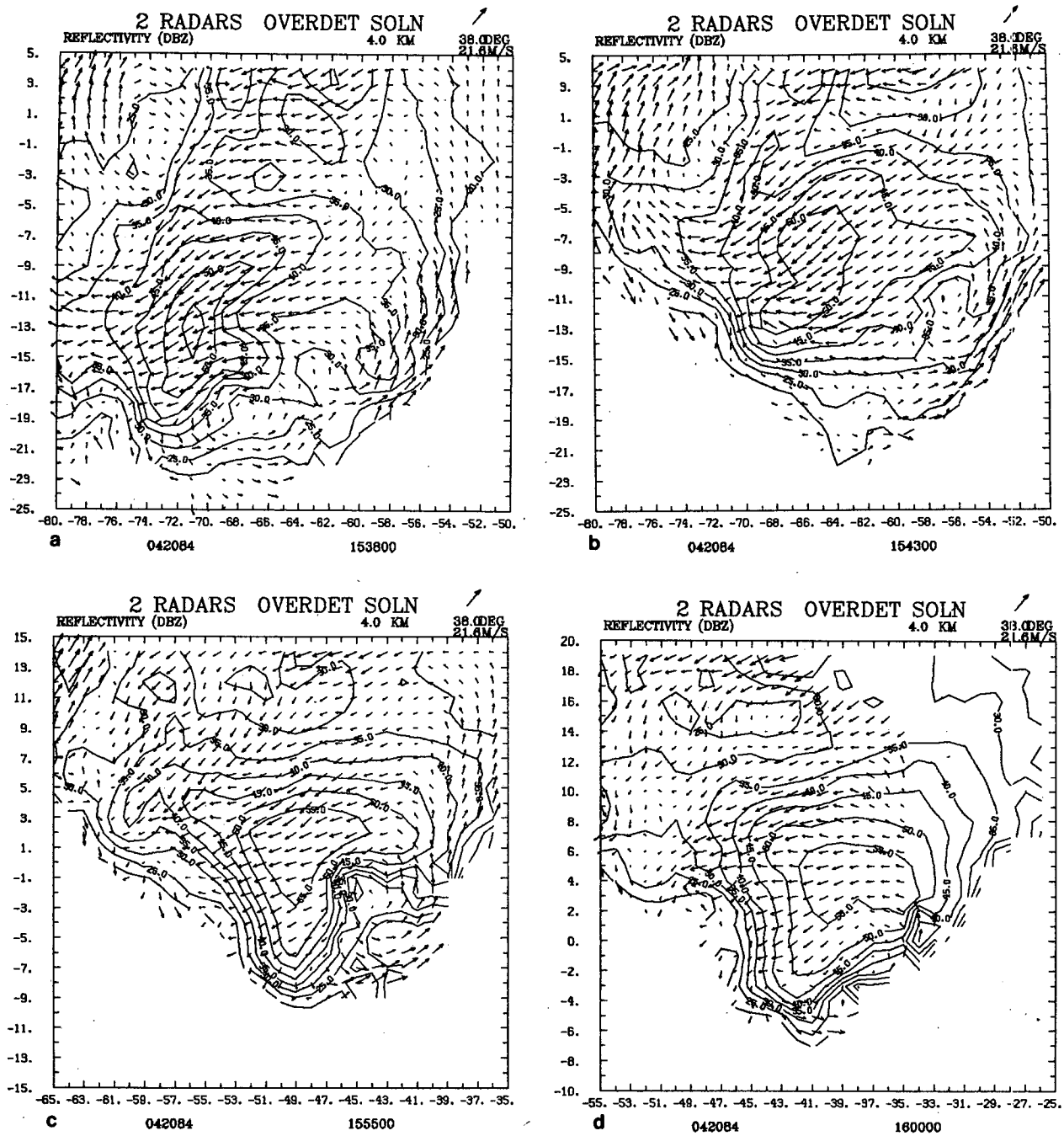

FIG. 3. Reflectivity and horizontal flow field for ground-based dual-Doppler analysis. Times are (a) 1538, (b) 1543, (c) 1555, (d) 1600, (e) 1607, and (f) 1612 CST. Height of analysis is 4.0 km. Calibration vector length is given with the storm motion vector in the upper right corner of each plot. Axes are in km and the Norman and Cimarron radar locations are at coordinates (0.0, 0.0) and (31.7, 26.6) km, respectively.

the scanning mode of one of the radars and the storms proximity to the Cimarron Doppler, the available wind fields cover only a small area at the time of most interest. This is an example of one situation where airborne Doppler radar can be useful.

The dual airborne (Fig. 6) and combination ground-based and airborne (Fig. 4) analyses shown are close to the times of the last ground-based analysis presented (Fig. 3f). The maximum reflectivity values and their location are in general agreement with the ground-based results. The structure of the reflectivity features also corresponds fairly well among the three different

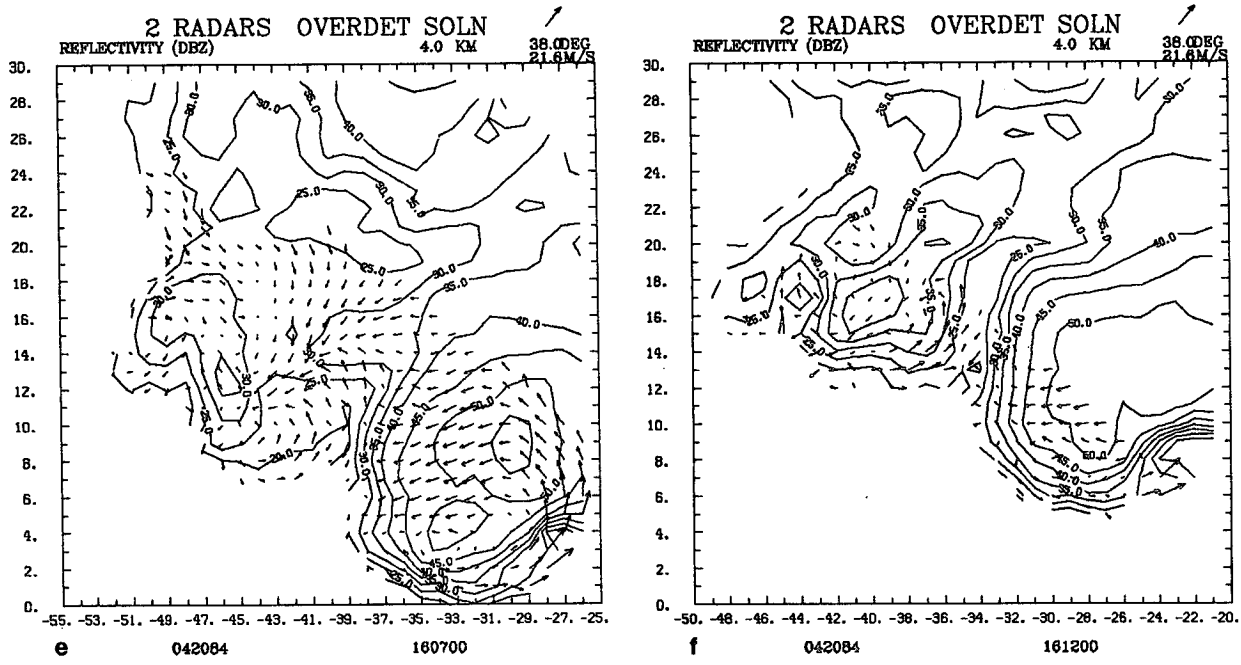

FIG. 3. (*Continued*)

analyses. The two reflectivity maxima and the strong gradient between them is present in all three analyses.

The developing hook echo and associated cyclonic circulation can clearly be seen in the combined airborne and ground-based analysis (Fig. 4). The hook feature is evident in the dual-airborne reflectivity (Fig. 6), but the wind fields are not available in the region of interest due to the placement of the fifth flight leg. The analysis which combined that last three flight legs (Fig. 7) exhibits the same general features as seen in the other

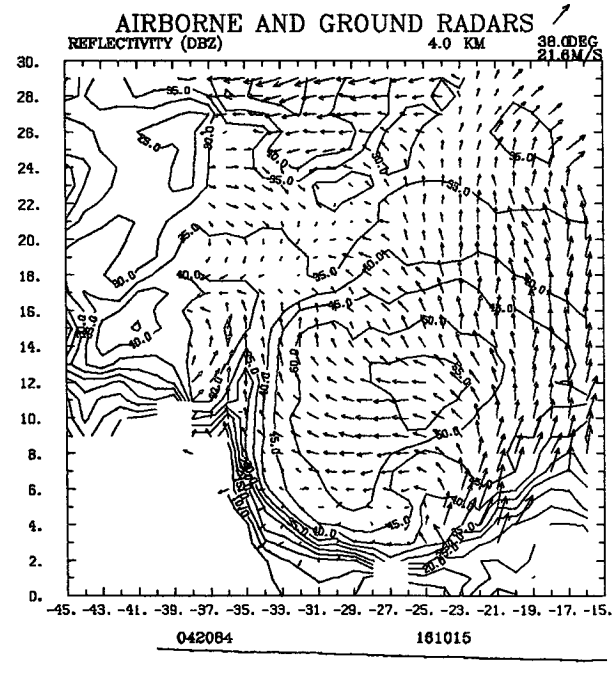

FIG. 4. Reflectivity and horizontal flow field for a combination airborne (leg 6) and ground-based (Norman) radar data for 1610:15 CST. Height is 4.0 km.

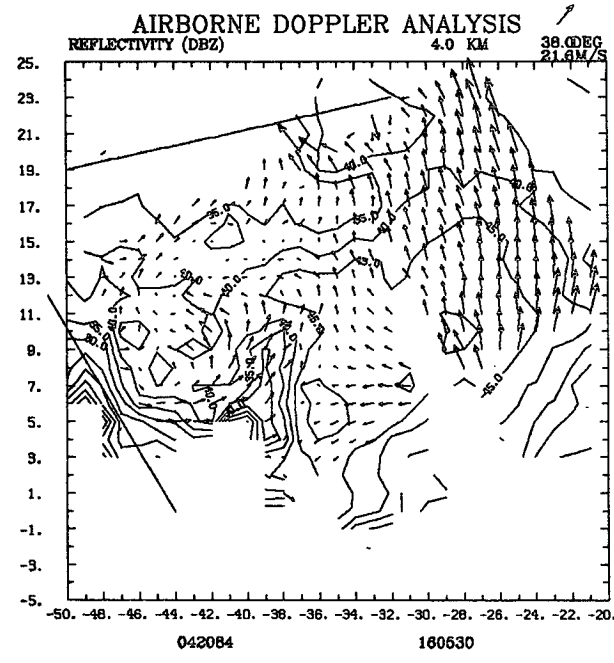

FIG. 5. Reflectivity and horizontal flow field for dual airborne analysis (legs 4 and 5) for 1605:30 CST. Height is 4.0 km. Axes are in km.

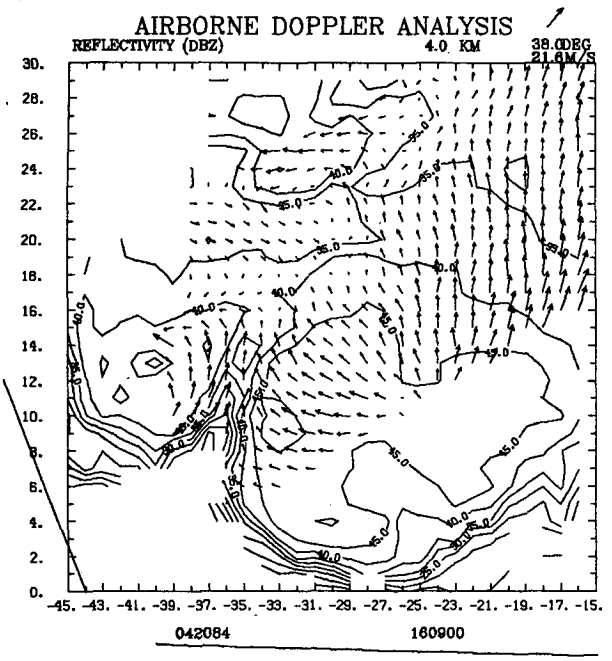

FIG. 6. Reflectivity and horizontal flow field for dual airborne analysis (legs 5 and 6) for 1609 CST. Height is 4.0 km and axes are in km.

results for that time. The magnitude of the reflectivity features is somewhat smaller, most likely due to attenuation of the 3-cm wavelength airborne Doppler radar. This 3-leg analysis also has a problem of missing winds due to the short length of the fifth leg.

The vertical velocity fields for the ground-based analyses at 1607 and 1612 CST point out the problems with the ground-based data collection at those times. The area that was observed by both radars was very small, resulting in little useful data at a time when the storm was at an important stage in its development. The whole lower right corner of the analysis grid is only observed by one of the legs. The combination of Norman and leg 6 provides the best areal coverage of data. Weak vertical velocities predominate over much of the analysis domain at 4 km height and 1605:30 CST. Near the flight leg, where vertical velocity estimates are unreliable, a strong updraft is indicated. A strong downdraft is observed in the area of the cyclonic circulation. The addition of the third leg increases the area which could be analyzed. Even though the length of data collection has been extended by about 3.5 minutes, the most interesting part of the storm is still not covered due to the length and geometrical configuration of the flight legs.

6. Synthesis uncertainties

a. Uncertainties due to geometry

Significant uncertainties that can be attributed to geometric effects are usually related to scans that involve high elevation angles (>20°) and/or scans close to the radar baseline. The other extreme is for attempted synthesis at long distances, which is a rarely observed problem. Geometrically induced uncertainties can be significant for airborne Doppler radar synthesis. Here, the expected sensitivity of the synthesis to geometry is examined for the wind fields presented in Figs. 3–7. Figure 8 shows the standard deviation of the expected error (in m s^{-1}). To aid in the interpretation, all the illustrations in Fig. 8 are for the vertical velocity at 4 km height. Radial velocity uncertainties are normalized at the grid locations to ease in scaling the resulting fields. Figure 8a is for just the two ground-based Doppler radars. One radar was located at coordinates (0.0, 0.0) and the other at (−31.7, 26.6), so that the radar baseline ran northwest–southeast past the northeast corner of the grid. The analysis time is about 1607 CST. It is clear that the best vertical velocities (and horizontal velocities) should be toward the south, with increasing uncertainty toward the northeast. The radar synthesis program checks for geometrically induced uncertainties and does not produce winds in regions where they would be unreliable. Thus, in Fig. 3e, there are reflectivities, but no velocities in the northeast portion of the grid.

This problem is reduced when the data from an approximately east–west leg is used with the Norman (0.0, 0.0) radar for data collected near 1610 CST. The expected impact of geometry is illustrated in Fig. 8b. Large errors are expected close to the flight track, but the expected uncertainties are small over most of the

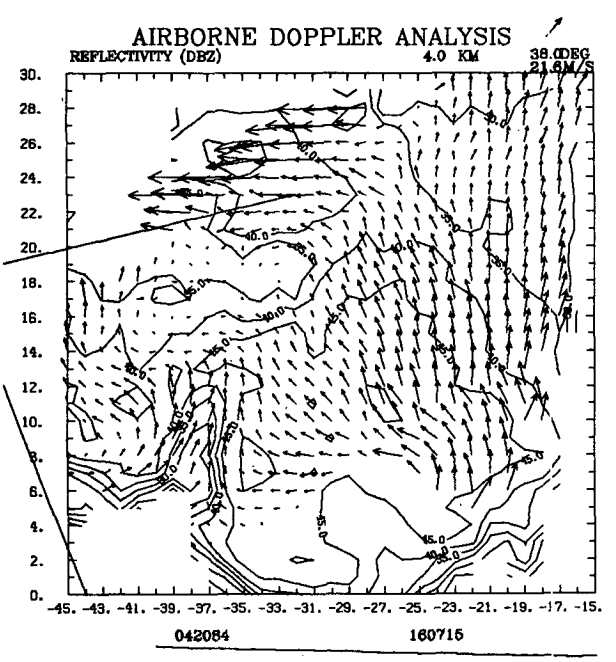

FIG. 7. Reflectivity and horizontal flow field for a triple airborne analysis (legs 4, 5, and 6) for 1607:15 CST. Height is 4.0 km and axes are in km.

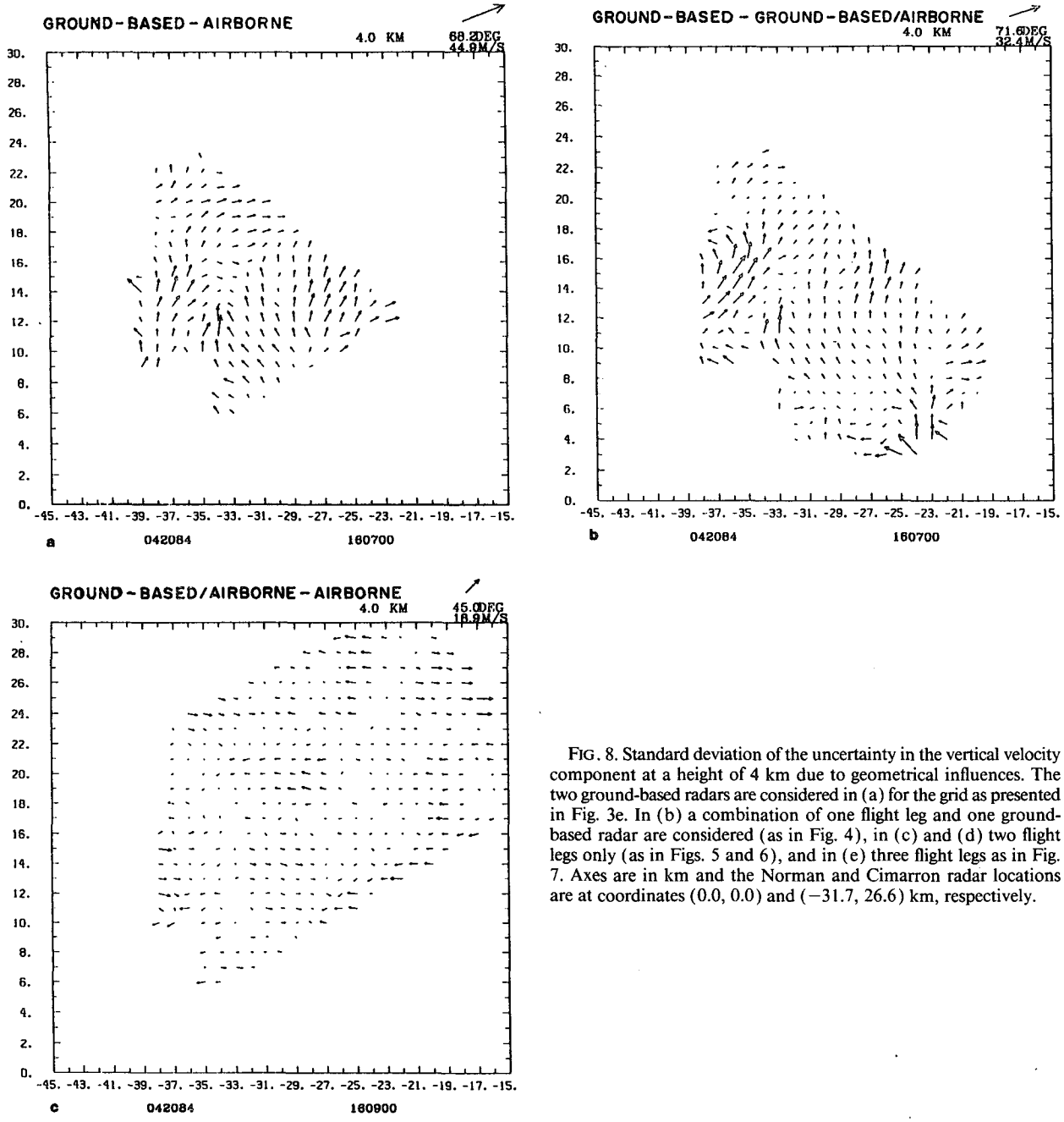

FIG. 8. Standard deviation of the uncertainty in the vertical velocity component at a height of 4 km due to geometrical influences. The two ground-based radars are considered in (a) for the grid as presented in Fig. 3e. In (b) a combination of one flight leg and one ground-based radar are considered (as in Fig. 4), in (c) and (d) two flight legs only (as in Figs. 5 and 6), and in (e) three flight legs as in Fig. 7. Axes are in km and the Norman and Cimarron radar locations are at coordinates (0.0, 0.0) and (−31.7, 26.6) km, respectively.

analysis domain. Notice that the use of airborne data allowed the synthesis to be extended to the region between the radars, which would otherwise not be represented. As suggested by the error analysis, the wind-field synthesis in Fig. 4 shows no evidence of large errors.

Airborne Doppler synthesis is considered without ground-based Doppler radars in Fig. 8c. At least two flight legs are required for synthesis. This figure relates to Fig. 5, and the data was acquired around 1605 CST. Data in Fig. 5 exists beyond the boundaries suggested in Fig. 8c because (i) the actual flight path is not an exact straight line and the data is placed according to the actual antenna position and not its approximate position, and (ii) data are translated to new positions in accordance with the difference between the time the data was collected and the synthesis time. The errors to the west and north in the synthesis domain are expected to be substantially larger than those in the southeast corner. An examination of the velocities in Fig. 5 indicates that the winds in the eastern portion of the domain are better (compare to Fig. 4) and that

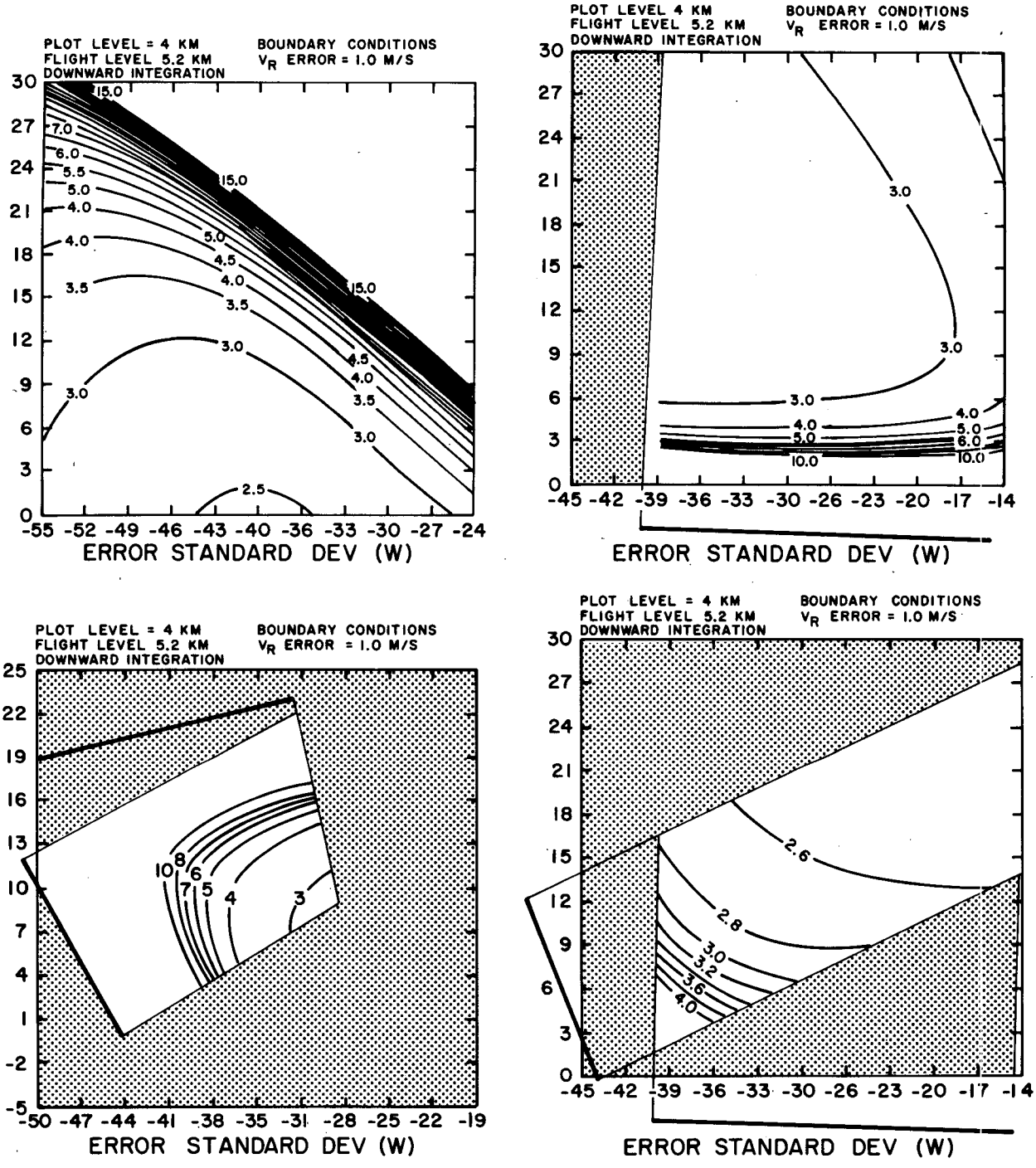

FIG. 9. Difference field for (a) dual ground-based minus dual airborne, (b) dual ground-based minus combination of ground and airborne, and (c) combination of ground and airborne minus dual airborne at 4.0 km height. Times for (a) and (b) are 1607, and for (c), 1609 CST. Axes are in km and the Norman and Cimarron radar locations are at coordinates (0.0, 0.0) and (−31.7, 26.6) km, respectively.

the winds in the northern section seem to deviate substantially from those of the airborne/ground-based radar combination.

When anotherpair of legs is used, as in Fig. 8d, a different distribution of uncertainties results. For these legs, centered about the 1609 CST analysis time, uncertainty decreases toward the northeast. Indeed, the synthesis appears close to that in Fig. 4, although it must be kept in mind that both syntheses used data from a common leg.

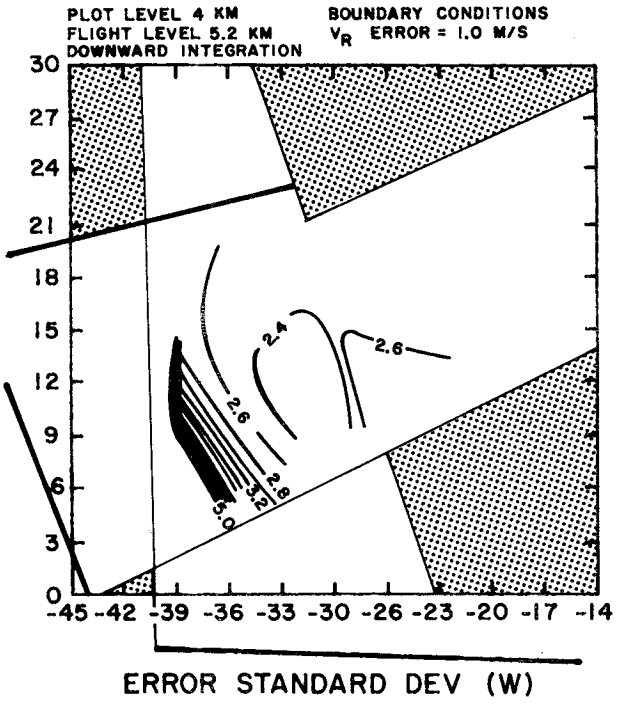

FIG. 9. (*Continued*)

When data from three legs are combined as in Fig. 7, the resulting uncertainties are everywhere smaller than they are from any subset of legs. The resulting uncertainties are illustrated in Fig. 8e. It is seen that the most northern leg contributes little to the reduction of uncertainty, partly since it is so nearly parallel to the east–west leg to the south. The area in the northern and southern portion of the domain contain regions of relatively high uncertainty as is evident in Fig. 7. Here, the magnitude of the east–west component of wind is poorly determined since the beams are oriented almost north–south from the radar when the data was being obtained from either leg. The rest of the differences are small, but perhaps significant. When considering using data from additional legs, it is important to consider the degree of independent information that is being received and the added uncertainty due to the increase in acquisition time and the effects of storm evolution.

b. Uncertainties due to temporal effects

If the storm were to simply translate with the wind, then the storm displacement could be found by maximizing the scalar correlation of the reflectivity field (as is customarily done), or the vector wind field, as presented in Eq. (6). All correlations were performed on the wind fields at 4.0 km height. For either scalar or vector correlations, with no evolution, the correlation will be 1.0. The departure from 1.0 can be attributed to evolution, and it might be further assumed that analyses with higher correlations contain less error from other sources, such as geometry. Finally, the difference field between two such correlated analyses will contain the minimum vector difference [as defined in Eq. (6)] in the wind field. Thus, the correlation between the ground-based and airborne analysis for the 1607 time (Figs. 3e and 6) was 0.63, while the correlation between the ground-based and airborne/ground-based analyses for the same time (Figs. 3e and 4) was 0.70. This expected result reflects the influence of the common ground-based radar data. When data from a single ground-based radar is added to a single leg of data collected by the airborne Doppler (Figs. 4 and 6), the correlation is 0.76.

Examining the correlation coefficients for the all the ground-based analyses from 1538 to 1638, the average value between successive times is 0.65. Ground-based radar took an average of 5 minutes to collect their volume scans. Although geometrical effects undoubtedly contribute to a reduced correlation, evolution limits the degree to which fields can be related.

The field that contain airborne data (Figs. 4 and 6) contain much larger winds from the south at the western and southeastern edges of the storm than the field derived from ground-based data alone (Fig. 3e). These differences are seen in Figs. 9a and 9b. The comparison between analyses that contain airborne data show much smaller and less systematic differences (Fig. 9c).

Approximately ten minutes were required to collect the data for airborne synthesis of wind fields. The correlation between successive ground-based syntheses spaced approximately that far apart is about 0.65. If the difference in ground-based syntheses is attributed to changes in the wind field over that period of time, and not, for example, to changes in orientation of the storm with respect to the radar network, then the airborne Doppler synthesis that extends over a comparable period cannot do better. Based upon these results, the evolution effects suggest this rapidly evolving storm would introduce root-mean-square errors of order 4 m s^{-1} to the airborne synthesis. This is based upon the assumption that airborne synthesis differs from ground-based only in the difference in the collection time required, i.e., the geometry induced uncertainties are small. These results are summarized in Table 1.

TABLE 1. Correlation coefficients.

Data type	Time	Correlation coefficient
Ground-based and airborne	1607	0.63
Ground-based and airborne/ground-based	1607	0.70
Single ground-based and single airborne	1607	0.76
Average ground-based	1538–1638	0.65

7. Discussion

There are several potential advantages in the use of airborne Doppler radars. They are able to observe storms where ground-based radars cannot, they are able to observe rapidly moving storms over their entire evolution, and they can take measurements of large storms in relatively short periods of time. Airborne Dopplers can be used to augment coverage by ground-based radars. Combining airborne and ground-based observations of a storm can increase the area of coverage and substantially reduce the amount of time necessary to observe the entire storm. Through proper selection of flight tracks, uncertainties due to sampling geometry can be minimized. Airborne Dopplers also can provide better spatial resolution than ground-based Dopplers. In the case discussed in this paper, the airborne Doppler data was seen to improve significantly coverage in an area where the ground-based radars did not provide suitable data.

The length of time required for each flight leg is generally a problem with airborne Doppler data. If the data collection takes too long, the temporal effects can degrade the analysis results. Good analyses using combinations of flight legs require the data to be somewhat stationary during the analysis period. This is particularly a problem when combining more than two flight legs. However, each flight leg in the dataset used here was only 2 to 2.5 minutes long. This means data collection for the airborne radar cases are about 5 minutes, about the same as that for the ground-based radars. These flight leg times were shorter than much of the airborne Doppler data analyzed previously. The short flight legs contributed to the quality of the airborne Doppler analyses.

Obviously, attenuation can be a serious problem when using airborne Dopplers to observe convective storms. The effects of attenuation are apparent when Figs. 4 and 6 are compared. The reflectivity fields in both figures are the maximum observed reflectivity at each grid point. The combined airborne and ground-based Doppler analysis shows the influence of the Norman Doppler. This field more closely resembles the dual ground-based Doppler analysis than does the dual-airborne analysis. Attenuation causes a decrease in magnitude of the reflectivity field and a distortion in the shape of the reflectivity field around the highest reflectivity values. The overall agreement in reflectivity fields (intensity and location) between the ground-based dual Doppler analyses and the airborne dual-Doppler analyses was found to be quite good. The most notable differences were due to the attenuation of the airborne Doppler radar beam. This high attenuation rate of the airborne Dopplers means that combining airborne with ground-based data may give better results than using airborne data alone. The reflectivity fields of the airborne Dopplers were good enough, despite their attenuation, to be worth using both by themselves and in combination with ground-based fields.

The analysis techniques used in this paper essentially weighted the ground-based radars less than the airborne Dopplers. As a result, the largest contribution of the airborne Doppler data was the increase in coverage of the storm. This was particularly important in this case, and should not be ignored as a reason to use airborne Doppler. Different weighting methods need to be explored in order to further investigate the effects of combining airborne data with ground-based data.

One disadvantage of the airborne Doppler data is the small Nyquist velocity (12.7 m s^{-1}). The amount of editing required to remove all of the velocity folding was quite substantial. As a result, the airborne data needed much more preprocessing than did the ground-based data.

The geometrical configuration of the flight path is an important consideration in airborne Doppler analysis. Without the proper configuration, the data can be useless. The "box" pattern of flight legs at right angles to each other is a good way to get independent estimates of a storm. This proved to be a good configuration for this dataset except that one leg was shorter than desirable. The loss of just a few kilometers on one leg meant losing data on the most interesting part of the storm being observed.

Overall, the addition of the airborne Doppler dataset to the data collected on this storm was seen to be very useful. The aircraft was able to sample the entire storm fairly rapidly. The storm went through an area of dual ground-based Doppler coverage. Unfortunately, at a critical time in the storm's development, one of the radars did not collect suitable data. This problem was alleviated by the airborne Doppler coverage at that time. Due to the configuration of the flight path, the airborne Doppler also missed some crucial data, which was observed by one of the ground-based Dopplers. The combination of one ground-based Doppler radar with one flight leg was seen to solve both of these problems.

Acknowledgments. The authors acknowledge the help of Dr. Kenneth Johnson of the Florida State University Supercomputer Computations Research Institute. A substantial portion of this work was completed as partial fulfillment of the degree requirements for M. Stephenson's Masters degree from the University of Oklahoma. This work was partially supported by NSF Grant ATM-8403452 to the University of Oklahoma and By NSF Grants ATM-8604143 and ATM-8619957 and NOAA Grant 40RANR608326 to the Florida State University. Partial support was also provided by Department of Energy Contract DE-FC05-85ER250000 to the Florida State University Supercomputer Computations Research Institute.

REFERENCES

Hildebrand, P. H., and C. K. Mueller, 1985: Evaluation of meteorological airborne Doppler radar. Part I: Dual-Doppler analyses of air motions. *J. Atmos. Oceanic Techonol.*, **2**, 362–380.

Jorgensen, D. P., P. H. Hildebrand and C. L. Frush, 1983: Feasibility test of an airborne pulse-Doppler meteorological radar. *J. Climate Appl. Meteor.*, **22,** 744–757.

Joss, J., and A. Waldvogel, 1970: Raindrop size distribution and Doppler velocities *Preprints 14th Radar Meteorology Conference,* Tucson, Amer. Meteor. Soc., 153–156.

Lamberth, R. L., 1966: On the use of Court's versus Durst's techniques for computing vector correlations coefficients. *J. Appl. Meteor.*, **5,** 736–737.

Lhermitte, R. M., 1971: Probing of atmosphere motion by airborne pulse-Doppler radar techniques. *J. Appl. Meteor.*, **10,** 234–246.

Marks, F. D., and R. A. Houze, 1987: Inner core structure of Hurricane Alicia from airborne Doppler radar observations. *J. Atmos. Sci.*, **44,** 1296–1317.

Mueller, C. K., and P. H. Hildebrand, 1985: Evaluation of meteorological airborne Doppler radar. Part II: Triple-Doppler analyses of air motions. *J. Atmos. Oceanic Techol.*, **2,** 381–392.

Ray, P. S., and K. L. Sangren, 1983: On multiple-Doppler radar network design. *J. Climate Appl. Meteor.*, **22,** 1444–1453.

——, and D. P. Jorgensen, 1988: Uncertainties associated with combining airborne and ground-based Doppler radar data. *J. Atmos. Oceanic Technol.*, **5,** 177–196.

——, —— and S. L. Wang, 1985: Airborne Doppler radar observations of a convective storm. *J. Climate Appl. Meteor.*, **24,** 687–698.

——, C. L. Ziegler, W. Bumgarner and R. J. Serafin, 1980: Single- and multiple-Doppler radar observations of tornadic storms. *Mon. Wea. Rev.*, **108,** 1607–1625.